Vehicle System Dynamics: International Journal of Vehicle Mechanics and Mobility

Publication details, including instructions for authors and subscription information:
http://www.tandfonline.com/loi/nvsd20

A numerical model of a HIL scaled roller rig for simulation of wheel-rail degraded adhesion condition

Roberto Conti [a], Enrico Meli [a], Luca Pugi [a], Monica Malvezzi [b], Fabio Bartolini [a], Benedetto Allotta [a], Andrea Rindi [a] & Paolo Toni [a]

[a] Department of Energy Engineering, University of Florence, via S. Marta n. 3, 50139, Firenze, Italy

[b] Department of Information Engineering, University of Siena, via Roma n. 56, 53100, Siena, Italy

Available online: 21 Dec 2011

To cite this article: Roberto Conti, Enrico Meli, Luca Pugi, Monica Malvezzi, Fabio Bartolini, Benedetto Allotta, Andrea Rindi & Paolo Toni (2012): A numerical model of a HIL scaled roller rig for simulation of wheel-rail degraded adhesion condition, Vehicle System Dynamics: International Journal of Vehicle Mechanics and Mobility, 50:5, 775-804

To link to this article: http://dx.doi.org/10.1080/00423114.2011.640402

Vehicle System Dynamics
Vol. 50, No. 5, May 2012, 775–804

A numerical model of a HIL scaled roller rig for simulation of wheel–rail degraded adhesion condition

Roberto Conti[a], Enrico Meli[a], Luca Pugi[a], Monica Malvezzi[b]*, Fabio Bartolini[a], Benedetto Allotta[a], Andrea Rindi[a] and Paolo Toni[a]

[a]*Department of Energy Engineering, University of Florence, via S. Marta n. 3, 50139 Firenze, Italy;* [b]*Department of Information Engineering, University of Siena, via Roma n. 56, 53100 Siena, Italy*

(*Received 28 April 2011; final version received 3 November 2011*)

Scaled roller rigs used for railway applications play a fundamental role in the development of new technologies and new devices, combining the hardware in the loop (HIL) benefits with the reduction of the economic investments. The main problem of the scaled roller rig with respect to the full scale ones is the improved complexity due to the scaling factors. For this reason, before building the test rig, the development of a software model of the HIL system can be useful to analyse the system behaviour in different operative conditions. One has to consider the multi-body behaviour of the scaled roller rig, the controller and the model of the virtual vehicle, whose dynamics has to be reproduced on the rig. The main purpose of this work is the development of a complete model that satisfies the previous requirements and in particular the performance analysis of the controller and of the dynamical behaviour of the scaled roller rig when some disturbances are simulated with low adhesion conditions. Since the scaled roller rig will be used to simulate degraded adhesion conditions, accurate and realistic wheel–roller contact model also has to be included in the model. The contact model consists of two parts: the contact point detection and the adhesion model. The first part is based on a numerical method described in some previous studies for the wheel–rail case and modified to simulate the three-dimensional contact between revolute surfaces (wheel–roller). The second part consists in the evaluation of the contact forces by means of the Hertz theory for the normal problem and the Kalker theory for the tangential problem. Some numerical tests were performed, in particular low adhesion conditions were simulated, and bogie hunting and dynamical imbalance of the wheelsets were introduced. The tests were devoted to verify the robustness of control system with respect to some of the more frequent disturbances that may influence the roller rig dynamics. In particular we verified that the wheelset imbalance could significantly influence system performance, and to reduce the effect of this disturbance a multistate filter was designed.

Keywords: scaled roller-rig multi-body model; three-dimensional wheel–roller contact; adaptive filtering

*Corresponding author. Email: malvezzi@dii.unisi.it

ISSN 0042-3114 print/ISSN 1744-5159 online

http://dx.doi.org/10.1080/00423114.2011.640402
http://www.tandfonline.com

1. Introduction

Hardware in the Loop (HIL) testing of degraded adhesion conditions is an important tool for development and calibration of safety relevant on board subsystems like traction controls [1,2], odometry algorithms, WSP (wheel slide protection systems) [3]. HIL testing may be performed considering different levels of integration of the tested system with the surrounding vehicle as in the example of Firenze Romito MI-6 test rig [3]. More recently, in the research Centre of Firenze Osmannoro, Trenitalia has built an innovative full-scale roller rig in which it is also possible to simulate degraded adhesion conditions *in railway vehicle* according to a control scheme previously described in [4]. The control scheme proposed requires the on line estimation of the vehicle motor torque (to reduce the time of the setting up phase) by means of an estimator strategy that uses the roller angular velocity and the tangential component of the contact forces (measured on the support). Within this research activity, a scaled roller rig was designed and realised, with the aim of investigating the feasibility and the calibration of different control layouts that may be used also for the full-scale version [4,5]. In [5], the control laws for the definition of the roller torques and speeds were developed by means of considerations based on a simplified model that considered the system dynamics only in the longitudinal plane. The possible interactions between the longitudinal and lateral dynamics were not investigated.

In this paper, a numerical model of the scaled version of the roller rig is presented. The numerical model reproduces both the hardware (scaled bogie, rollers) and the software (simulated vehicle) parts of the roller rig. The main contribution of the paper is the study of the complete three-dimensional dynamics of the hardware part of the test rig, in particular, the contact between wheels and rollers [6] was modelled by adapting a previously existing algorithm, described in detail in [7,8], initially defined for the wheel/rail contact model: the algorithm was then modified to simulate the contact between two revolute surfaces and to work with variable step solvers (that improve the numerical efficiency and robustness). The software part of the roller rig and the control laws of the roller motors were derived substantially from those described in [4], even if some improvements were necessary: first of all, since the roller rig described in that paper tests a whole vehicle, while the scaled version tests only one bogie, the controller has to include a virtual vehicle, in which one of the bogies is real and the other is simulated. Furthermore, the roller motor control laws had to be modified taking into account the scaling factor. Since the same software environment (Matlab–Simulink) was used for the development of the real-time software of the scaled test rig (controller and virtual vehicle [4]), and the simulator of the hardware part of the test rig, the proposed study may be seen as a software in the loop (SIL) calibration of the control algorithms that will be directly compiled and implemented in the scaled rig.

In particular in this paper we investigated the robustness of the proposed control system with respect to some disturbances, for instance wheelset imbalance and bogie hunting. Furthermore the effect of simulated low adhesion conditions was evaluated. This sensitivity analysis was carried out by means of numerical simulations. The numerical control performance was evaluated in terms of angular speed error (between the simulated train model and the roller velocity) and torque estimation error (between the real torque and the estimated torque). The results show that the architecture proposed in [4] was robust in terms of angular speed error for both the scenarios while, as regards the dynamical imbalance disturbance, it was necessary to modify the estimation procedure. The proposed estimation strategy contains a multi-state nonlinear filter that consistently reduces the particular disturbance produced by the imbalance.

This paper is organised as follows: Section 2 summarises the general architecture of the scaled roller rig, Section 3 shows the developed multi-body simulator (and in particular

focuses on the wheel–roller contact model), while in Section 4 some numerical simulations are presented and discussed.

2. General architecture of the scaled roller rig

The main design features of the scaled roller rig [5], referred to as MDM roller rig in the following, are described in [4,9] and summarised here for the convenience of the reader. The railway bogie roller rig is used to reproduce on the test rig the train behaviour in degraded adhesion conditions. In order to reach this goal, HIL approach is used: a virtual *vehicle* model with a simplified adhesion model simulates the desired vehicle dynamics; then the test rig rollers are controlled in order to approximate the dynamical behaviour of the vehicle in terms of wheel angular velocity and vehicle motor torque. In [4], the feasibility of degraded adhesion tests on a HIL full scale roller rig is discussed.

This is the most important feature of the device, a reliable simulation of wheel sliding is necessary to test some on-board components and their interactions. This result could be obtained by reproducing, in the interface between the wheel and the rail, the same sliding that would be found during the real run of the vehicle, but this is not practically suitable for a number of reasons: the phenomena that arise in the wheel–roller interface are different from those arising in the wheel–rail interface, due to the geometry (the roll has a finite-curvature radius) and the environmental conditions; the sliding between the wheel and the roller may produce a significant wear on the roller profile; severe sliding tests may produce localised wear phenomena on the roller profile; this may lead to periodical disturbances that could heavily influence the test results. The design of the roller rig was then based on the idea that the sliding between the wheel and the rail is not reproduced in the wheel–roll interface, even when degraded adhesion conditions are met. In this case, the sliding is simulated by properly controlling the roller motor torques, that are regulated in order to obtain the same tangential force and the same wheel speed that exists between the virtual wheel and rail in the contact area. In other words, the sliding between the wheel and the rail is virtual.

A railway vehicle usually consists of two bogies, four wheelsets, one car body and the primary and secondary suspensions. The scaled roller rig described in this paper is designed to test only a single-scaled bogie and consequently, to simulate a whole vehicle, a second roller rig would be necessary: this second-scaled roller rig is implemented via software by means of a simplified analytic model. This strategy allows evaluation of the dynamical behaviour of the whole vehicle using a single-scaled roller rig and reducing the computational load.

The general architecture of the test rig is schematically shown in the block diagram of Figure 1.

The following main blocks can be identified in the scheme:

(1) *Scaled roller rig*: The scaled roller rig consists of two different elements, in order to simulate the whole railway vehicle roller rig:
   - *the MDM hardware scaled roller rig* [10]: it is composed of the scaled bogie and the actuated rollers. The scaled bogie includes the bogie body, two wheelsets and the primary and secondary suspensions.
   - *Virtual bogie roller rig*: The virtual bogie roller rig allows us to model the second bogie by means of a simplified analytic virtual model in order to simulate the whole railway vehicle.
   - *Virtual antiskid*: The antiskid modifies the torque erogation taking into account the adhesion limit.

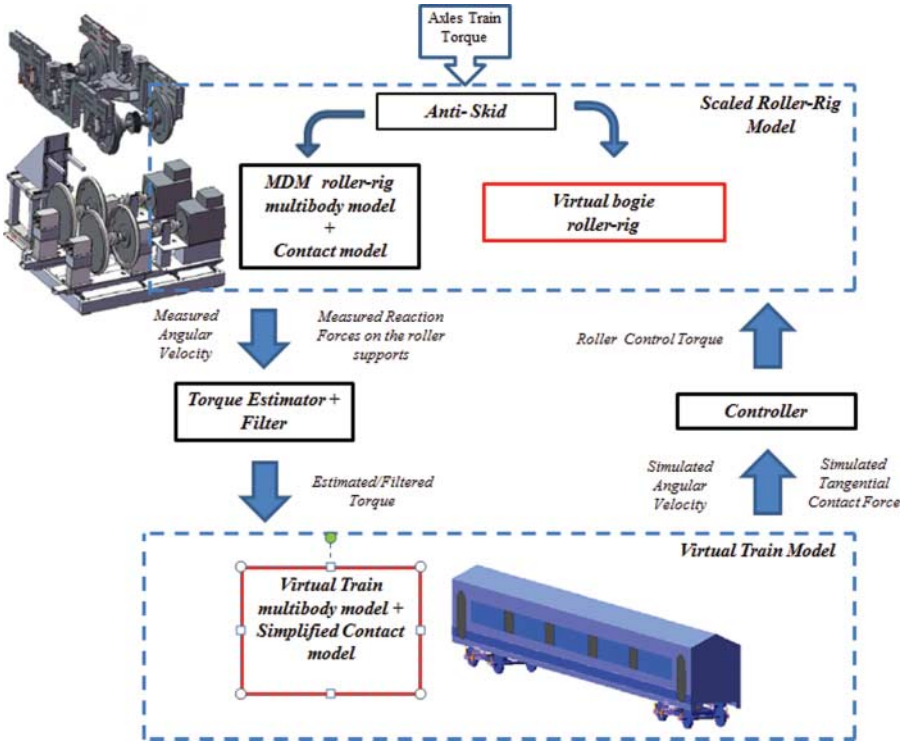

Figure 1. General architecture of the scaled roller rig.

(2) *Virtual train model*: it is the model of the vehicle used to simulate the locomotive behaviour on the rail in different adhesion conditions [1,2,4]. This multi-body model is a part of the roller-rig control system and then has to be designed for a real-time implementation: a simplified but realistic contact model is considered, that allows us to reproduce different adhesion conditions.
(3) *Controllers*: its task is to reproduce on the hardware roller rig the same dynamical behaviour of the virtual train model in terms of wheel angular velocity and vehicle motor torque [4,11].
(4) *Estimators/Filters*: The data which can be measured by the sensors installed on the MDM roller rig are the roller angular velocities and the reaction forces on the roller supports. This choice is mainly due to replication of the sensor structure that will be installed on the full-scale solution [4], in this case the tested vehicle will be a locomotive and in order to speed up the set up process, no sensors will be placed on it. The estimator block allows for evaluation of an estimation of the creep forces and of the wheel angular acceleration in order to calculate the estimation torque applied by the bogie motor on the wheelsets [4]. The filter block reduces the noises/disturbances (high-frequency noise, disturbance generated by the dynamical imbalance of the wheelset, etc.) on the estimated torque [12].

From the control point of view, the external input of the whole model is the torque applied to the wheels; this torque is unknown to the control system. The controlled parameter is the error between the virtual train angular velocities and the measured roller angular velocities. Since the wheelset torques are not directly measured, but are estimated, as described in [4] as a function of the sensor measures on the roller rig, the actual torque may be different from the estimated one.

As previously mentioned, to obtain a more realistic bogie dynamics, an antiskid device is simulated: the axle train torque is modulated starting from the knowledge of the virtual train dynamics in order to control the virtual sliding between the wheels and the rail.

The estimator/filter block, from the measures of the roller angular velocity and the tangential component of the contact forces, evaluates the estimated torque on the wheelset. The torque estimator includes filters that reduce the estimation error and the noises and disturbances (high-frequency noise, disturbance generated by the dynamical imbalance of the wheelset, etc.).

The virtual train model simulates the dynamic behaviour of the train in different conditions. The input of this model is the estimated/filtered torque on the wheelset and the output are the simulated angular velocities and the simulated tangential contact forces. To calculate these output values, a simplified contact model is employed. The controller block evaluates the torque to be applied on the rollers, in order to obtain on the roller rig the same angular velocities of the virtual train model.

In order to preliminarily evaluate the performance of the proposed control structure, a simulator of the whole test rig has been developed. The simulator includes the software part of the system and a three-dimensional multi-body model of the hardware part (the scaled bogie and the rollers). The whole system simulator has been implemented in the MATLAB®–Simulink® environment, in particular, the multi-body model has been implemented in the MATLAB® toolbox SimMechanics. The use of the MATLAB®–Simulink® environment allows us to consider many numerically efficient integration algorithms; moreover, the structure of the Simmechanics is modular and parametric and therefore particularly suitable for modelling complex multi-body systems.

3. The simulator of the scaled roller rig

In this section, the components of the roller rig simulator will be explained. In Figure 2, the detailed architecture of the model and the flow data between the blocks are shown. The model consists of two macroparts: the full-scale model and the scaled model; to connect these parts, some scaling blocks (containing the proper scaling factors) are needed. Throughout the paper, the apex 'sc' indicates the variables in the scaled model. From a logical point of view, the whole model can be split into four main sub-blocks: the scaled roller rig, the virtual train model, the controller and the sensor/estimator/filter. Figure 3 shows the 3D CAD model of the scaled roller rig and the realised prototype.

3.1. *Scaled roller rig*

3.1.1. *MDM roller rig: multi-body model*

The aim of this multi-body model is to simulate the dynamic behaviour of the MDM test rig. Some previous studies described the design of an MDM roller rig and the considered scaling hypothesis [4,5,10].

A proper definition of the similitude laws between the scaled model and the real full-scale system allows us to obtain realistic results and, at the same time to correctly interpret the experimental data. In literature different approaches are proposed [5]. For the MDM test rig, Iwnicki scaling method was chosen; this approach involves several consequences on the system which are as follows:

- *Time scaling*: it assures that no scaling is applied to elapsed time and system frequencies; this is a useful feature since the rig is dedicated to HIL simulation. This method allows us to maintain the same time and frequency behaviour both in the real system and the scaled one.

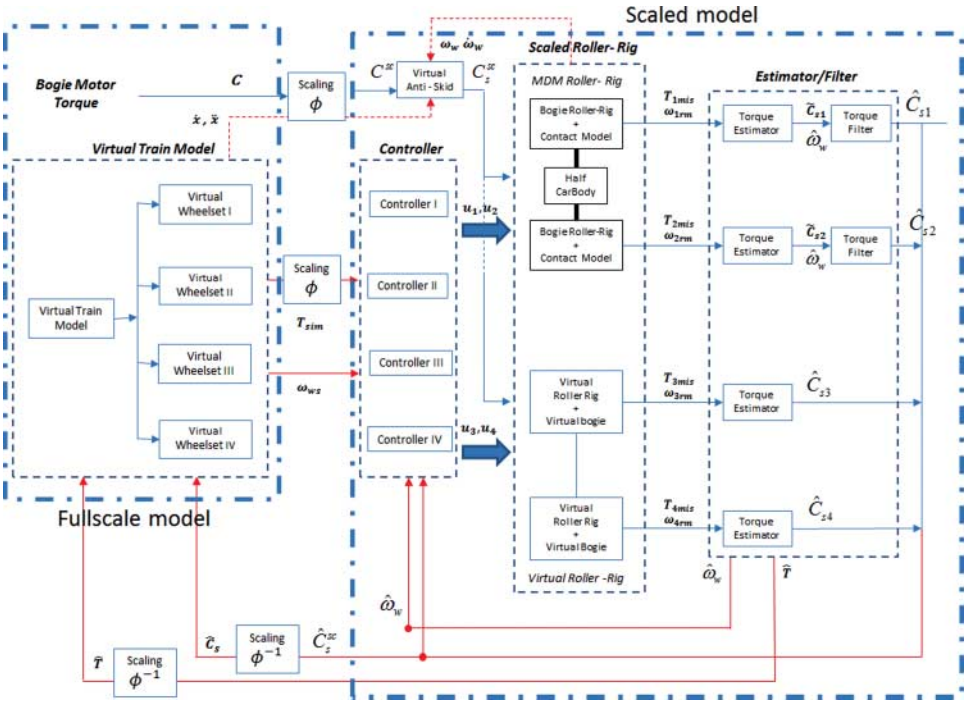

Figure 2. Detailed architecture.

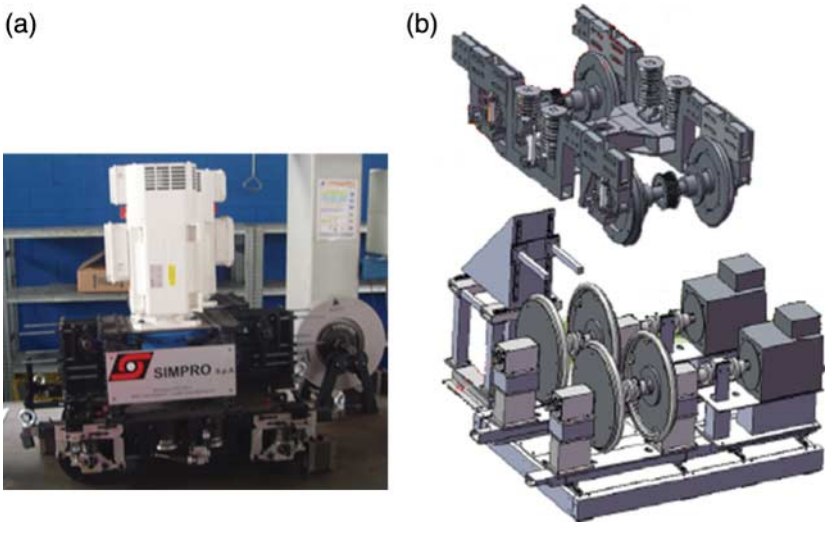

Figure 3. The MDM scaled roller rig, a) the scaled bogie, b) the 3D CAD model.

- *Mass–weight mismatch*: It introduces a different scaling factor for mass and weight. For the design of the mechanical part of the rig this is a problem, since weight is proportional to mass through the gravity acceleration. Actually in the presented case, this effect can be quite useful because it permits us to reduce the slidings on the interface between rollers and wheels.

Table 1. Iwnicki scaling method.

	Scaling factor
Length	$\phi_l = 5$
Time	$\phi_t = 1$
Velocity	$\phi_v = 5$
Acceleration	$\phi_a = 5$
Mass	$\phi_m = 125$
Force	$\phi_f = 625$
Density	$\phi_d = 1$
Young modulus	$\phi_y = 1$
Weight	$\phi_w = 125$
Stiffness	$\phi_s = 125$
Contact forces	$\phi_f = 625$
Damping	$\phi_d = 125$
Torque	$\phi_C = 3125$

The scaling factors calculated with the Iwnicki procedure are summarised in Table 1.

The three-dimensional multi-body model of the MDM roller rig presented in this paper is more accurate than those described in the previous works [8,10]. It consists of two parts: the scaled roller rig and the scaled vehicle (half vehicle, according to the architecture introduced before). The scaled roller rig consists of two rollers (two rigid bodies constrained to rotate around their axis) and a basement.

The scaled roller-rig parameters are detailed in some previous works [10]. The scaled vehicle multi-body model is composed of six rigid bodies: the half car body, the front bogie and two wheelsets. The wheelsets (six DoFs for body) are linked to the bogie only by three-dimensional nonlinear elastic-viscous force elements modelling the primary suspensions; the bogie (five DoFs) is constrained along the longitudinal direction (to avoid the fall from the roller rig) and it is linked to the half car body by three-dimensional nonlinear elastic-viscous force elements reproducing the secondary suspensions; finally in this particular case, the half car body is constrained to move only along the vertical axis (one DoF).

The effect of the wheelset unloading caused by the traction/braking phase has not been considered; this aspect of the problem (due to the coach pitch motion) will be investigated in the future when a complete three-dimensional model of both the scaled roller rigs will be available.

In this paper, the Manchester Wagon, whose physical and geometrical data can be easily found in literature [13], has been chosen as a benchmark vehicle. This choice is also precautionary because, since the Manchester bogie is lighter than a locomotive bogie, its dynamical effects are faster and more severe than those on the locomotive one. The scaled bogie dimensions are referred to this vehicle by means of properly scaling factors. Starting from these values, the MDM roller rig has been designed [10] according to the architecture previously presented. The maximum values of the roller angular velocity $\omega_w = 200$ rad/s and roller motor torque $C_S^{sc} = 20,000/\phi_C$ N m have been derived from practical considerations on the operative conditions of the considered devices, derived from some previous analysis conducted on a full-scale test rig and described in [10]. The first value derives from the maximum linear velocity to be simulated, while the second one was derived from the maximum torque of the motors of the full scale roller rig described in [3].

The dynamical axle imbalance values have been chosen according to the limits prescribed in [14].

In the MDM roller rig, the sensors whose measures are used by the controller are tri-axial load cells (which measure the reaction force on the rollers support) and the angular velocity

sensor of the roller. The angular wheel velocity, the angular wheel acceleration and the bogie motor torque are evaluated by an estimation procedure.

3.1.2. *Wheel/roller contact model*

The wheel/roller contact model is an improvement of previous models developed for the wheel–rail pair and detailed in [7,8]. The contact model can be logically divided into two parts: the contact point detection between two revolute surfaces and the calculation of the normal and tangential contact forces.

There are different strategies in literature [15–17] to find the contact points. Those adopted in the roller-rig simulator is based on a semi-analytical procedure and satisfies the following requirements:

- The contact detection algorithm between revolute surfaces is fully three-dimensional and does not introduce simplifying assumptions on the problem geometry and kinematics
- Generic wheel–roller profiles
- Accurate management of the multiple contact points without limits on the point number
- High computational efficiency needed for the online implementation within multi-body models

The research of the contact points is based on the consideration that the contact points between the wheel surface and the roller surface are located where the distance between the two surfaces assumes a stationary point. The following conditions allow us to find these points:

(1) *Parallelism condition* between the normal unitary vector to the roller surface and the normal unitary vector to the wheel surface
(2) *Parallelism condition* between the normal unitary vector to the roller surface and the vector representing the distance $\mathbf{d}^r$ between the generic point of the wheel and the rail surfaces.

Going through the details of the procedure, a fixed reference system $O_r x_r y_r z_r$ is defined, with its origin located on the roller rotation axis and the axis y_r parallel to the rotation axis (see Figure 4). The local reference system $O_w x_w y_w z_w$ is defined on the wheelset, with the axis y_w coincident with the rotation axis of the wheelset. The origin O_w coincides with the common point between the nominal rolling plane and the wheelset axis.

The vector $\mathbf{O}_w^r$ is the position of the local references system with respect to the fixed one and $[\mathbf{R}]$ is the rotation matrix that represents the relative orientations. In the local system the axle can be described by a revolution surface. The generative function is indicated with $w(y_w)$.

In the local reference frame, the position of a generic point of the wheel surface is described by the following analytic expression

$$\mathbf{p}_{\mathbf{w}}^{\mathbf{w}}(x_w, y_w) = [x_w y_w - \sqrt{w(y_w)^2 - x_w^2}]^{\mathrm{T}}, \tag{1}$$

while in the fixed reference system the same position is given by

$$\mathbf{p}_w^r(x_w, y_w) = \mathbf{O}_w^r + [\mathbf{R}]\mathbf{p}_w^w(x_w, y_w). \tag{2}$$

Similarly, the roller can be described by a revolution surface with respect to the fixed reference system (the generative function is indicated by $r(y_r)$, see Figure 4). The main difference with respect to the method presented in [7,8] is obviously the geometry of the contact bodies. Since the semianalytic methods are based on a preliminary algebraic simplification of the above introduced geometrical conditions and since the contact geometries have necessarily different

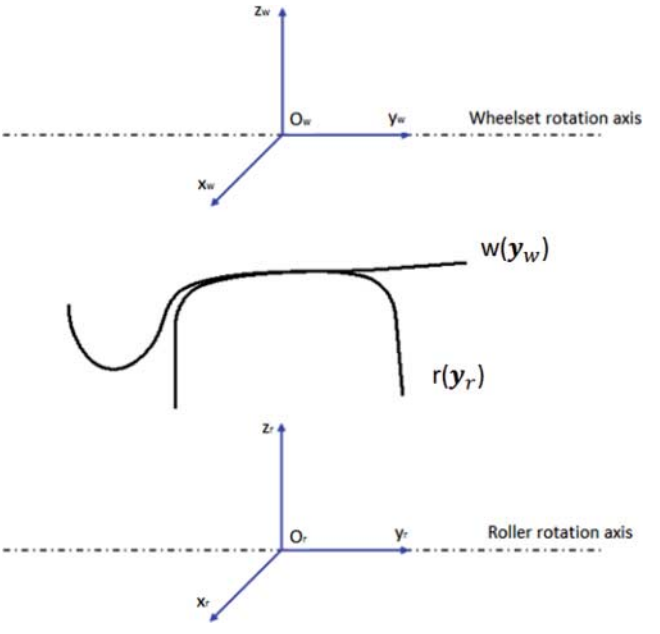

Figure 4. Fixed reference system – local reference system.

mathematical representations, the method presented in [7,8] has to be properly modified. The position of a generic point of the roller surface has the following analytic expression:

$$\mathbf{p}_{\mathbf{w}}^{\mathbf{r}}(x_w, y_w) = \mathbf{O}_{\mathbf{w}}^{\mathbf{r}} + [\mathbf{R}]\mathbf{p}_{\mathbf{w}}^{\mathbf{w}}(x_w, y_w). \tag{3}$$

The outgoing normal unit vector to the wheel surface in the local system is defined by $\mathbf{n}_w^w(\mathbf{p}_w^w)$, while in the fixed reference system, will be

$$\mathbf{n}_w^r(\mathbf{p}_w^r) = [\mathbf{R}]\mathbf{n}_w^w(\mathbf{p}_w^w). \tag{4}$$

In the fixed reference system, the outgoing normal unitary vector to the rail surface is defined as $\mathbf{n}_r^r(\mathbf{p}_r^r)$. The complete expressions of the normal unit vectors are

$$\mathbf{n}_w^w(\mathbf{p}_w^w) = \frac{-(\partial \mathbf{p}_w^w/\partial x_w \times \partial \mathbf{p}_w^w/\partial y_w)}{\|\partial \mathbf{p}_w^w/\partial x_w \times \partial \mathbf{p}_w^w/\partial y_w\|}, \quad \mathbf{n}_r^r(\mathbf{p}_r^r) = \frac{(\partial \mathbf{p}_r^r/\partial x_r \times \partial \mathbf{p}_r^r/\partial y_r)}{\|\partial \mathbf{p}_r^r/\partial x_r \times \partial \mathbf{p}_r^r/\partial y_r\|}. \tag{5}$$

The distance vector between two generic points belonging to the wheel surface and the roller surface is defined as

$$\mathbf{d}^r(x_w, y_w, x_r, y_r) = \mathbf{p}_w^r(x_w, y_w) - \mathbf{p}_r^r(x_r, y_r), \tag{6}$$

as can be seen, the distance vector is a function of four parameters.

The *Parallelism Conditions* can be formally written as follows:[1]

$$\mathbf{n}_r^r(\mathbf{p}_r^r) \parallel \mathbf{n}_w^r(\mathbf{p}_w^r) \longrightarrow \mathbf{n}_r^r(\mathbf{p}_r^r) \times [\mathbf{R}]\mathbf{n}_w^w(\mathbf{p}_w^w) = \mathbf{0}, \tag{7}$$

$$\mathbf{n}_r^r(\mathbf{p}_r^r) \parallel \mathbf{d}^r \longrightarrow \mathbf{n}_r^r(\mathbf{p}_r^r) \times [\mathbf{R}]\mathbf{d}^r = \mathbf{0}. \tag{8}$$

The conditions defined in Equations (7) and (8) are an algebraic system of six equations (of which only four are independent; for example, the first two components of each vectorial

equation) in four unknowns. However, as will be shown in the following, the original four-dimensional system can be analytically reduced to one single scalar equation $F(y_w) = 0$ (that, at this point, can be easily solved numerically) by expressing the variables x_w, x_r and y_r as a function of y_w.

The solutions of Equations (7) and (8) have to be checked in order to avoid the physical meaningless solutions. The first condition to check is the *indentation condition*. The *i*th solution x_{wi}^C, y_{wi}^C, x_{ri}^C, y_{ri}^C ($\mathbf{p}_{wi}^{r,C}$,$\mathbf{p}_{ri}^{r,C}$ in terms of contact points) can be accepted only if the indentation between the wheel surface and the roller surface is negative (with respect to the adopted convection):

$$p_{ni} = \mathbf{d}_i^{r,C} \cdot \mathbf{n}_r^r(\mathbf{p}_{ri}^{r,C}) \leq 0, \tag{9}$$

where $\mathbf{n}_r^r(\mathbf{p}_{ri}^{r,C})$ is the outgoing normal unitary vector to the roller surface in the candidate solution and $\mathbf{d}_i^{r,C}$ is the distance between $\mathbf{p}_{wi}^{r,C}$ and $\mathbf{p}_{ri}^{r,C}$. Otherwise, the solution must be rejected.

The *i*th solution has also to satisfy the *convexity condition*. This condition constrains the curvature radii of the roller profile to be smaller than the curvature radii of the wheel profile.

The complete expression of surface curvatures is described in [8]. Finally, the solutions with algebraic multiplicity larger than one have to be reduced to an unique solution rejecting the physical meaningless solutions. As said before, the four-dimensional problem can be reduced to a one-dimensional scalar problem expressing the variables x_w, x_r and y_r as a function of y_w. In order to determine x_w as function of y_w, the quantity $x_r/\sqrt{r(y_r)^2 - x_r^2}$ can be expressed as a function of x_w,y_w both from the second components of Equations (7) and (8): $x_r/\sqrt{r(y_r)^2 - x_r^2} = f_1(x_w, y_w)$, $x_r/\sqrt{r(y_r)^2 - x_r^2} = f_2(x_w, y_w)$. Comparing the two expressions, the following equation can be found:

$$B\sqrt{A^2 - x_w^2} = Cx_w - D, \tag{10}$$

where

$$A = w(y_w), \tag{11}$$

$$B = -G_x r_{33} - y_w r_{12} r_{33} + w(y_w)w'(y_w) r_{13} r_{32} + G_z r_{13} + y_w r_{13} r_{32} - w(y_w)w'(y_w) r_{12} r_{33}, \tag{12}$$

$$C = w(y_w)w'(y_w) r_{11} r_{32} + G_z r_{11} + y_w r_{11} r_{32}, \tag{13}$$

$$D = -G_x w(y_w)w'(y_w) r_{32} + G_z w(y_w)w'(y_w) r_{12}, \tag{14}$$

r_{jk} is the generic element of the rotation matrix [**R**], w' is the wheel profile derivative and G_x, G_y and G_z are the components of $\mathbf{O_w^r}$. The solutions of Equation (10) define the x_w as a function of y_w (there are two values of x_w for each value of y_w):

$$x_{w1,2}(y_w) = \frac{CD \pm \sqrt{C^2D^2 - (C^2 + A^2)(D^2 - A^2B^2)}}{C^2 + A^2}. \tag{15}$$

At this point, $x_r/\sqrt{r(y_r)^2 - x_r^2} = f_1(x_{w1,2}(y_w), y_w)$ that is only function of y_w, can be related to the quantity in $r(y_r)/\sqrt{r(y_r)^2 - x_r^2}$ because:

$$\frac{r(y_r)}{\sqrt{r(y_r)^2 - x_r^2}} = \sqrt{1 + \left(\frac{x_r}{\sqrt{r(y_r)^2 - x_r^2}}\right)^2}; \tag{16}$$

therefore, also $r(y_r)/\sqrt{r(y_r)^2 - x_r^2} = f_3(y_w)$ will be only a function of y_w. Subsequently, to determine y_r as a function of y_w Equation (16) can be inserted into the first component of the

vectorial equation (7):

$$r'(y_r)_{1,2} = -(f_3(y_w))^{-1} \cdot \frac{x_{w1,2}(y_w)r_{21} - w(y_w)w'(y_w)r_{22} - r_{23}\sqrt{w(y_w)^2 - x_{w1,2}(y_w)^2}}{-w(y_w)w'(y_w)r_{32} - r_{33}\sqrt{w(y_w)^2 - x_{w1,2}(y_w)^2}}. \quad (17)$$

Usually the function $r'(y_r)$ has a monotonic descending trend, therefore it can be numerically inverted in order to obtain $y_{r1,2}(y_w)$; if $r'(y_r)$ is not monotonic descending, the function can still be inverted but a further multiplication of the solution number is needed.

From the second component of Equations (7) and (16), $x_{r1,2}(y_w)$ can be calculated as a function of y_w:

$$x_{r1,2}(y_w) = \frac{r(y_{r1,2}(y_w))}{f_3 y_w} \cdot \frac{G_x + x_{w1,2}(y_w)r_{11} + y_w r_{12} - r_{13}\sqrt{w(y_w)^2 - x_{w1,2}(y_w)^2}}{G_z + y_w r_{32} - r_{33}\sqrt{w(y_w)^2 - x_{w1,2}(y_w)^2}}. \quad (18)$$

Finally, replacing the first component of Equation (8) the relations $x_{w1,2}(y_w), y_{r1,2}(y_w), x_{r1,2}(y_w)$ and the following scalar equation can be obtained where the unique unknown is y_w:

$$\begin{aligned} F_{1,2}(y_w) = &-r'(y_{r1,2})r(y_{r1,2})\left(G_z + y_w r_{32} - r_{33}\sqrt{w(y_w)^2 - x_{w1,2}^2} - \sqrt{r(y_r)^2 - x_r^2}\right) \\ &- \sqrt{r(y_{r_{1,2}})^2 - x_r^2}\left(G_x + x_{w1,2}r_{11} + y_w r_{12} - r_{13}\sqrt{w(y_w)^2 - x_{w1,2}^2 - y_r}\right) = 0. \end{aligned} \quad (19)$$

Replacing the solutions y_{wi}^C of the scalar equations $F_1(y_w) = 0$ and $F_2(y_w) = 0$ in Equations (15), (17) and (18) the values of the other variables can be obtained:

$$(x_{wi}^C, y_{wi}^C, x_{ri}^C, y_{ri}^C), \quad i = 1, 2, \ldots, n \quad (20)$$

and consequently the positions of the corresponding contact points on the wheel and on the roller:

$$\mathbf{p}_{wi}^{r,C} = \mathbf{p}_w^r(x_{wi}^C, y_{wi}^C), \mathbf{p}_{ri}^{r,C} = \mathbf{p}_r^r(x_{ri}^C, y_{ri}^C), \quad i = 1, 2, \ldots, n. \quad (21)$$

Since Equation (10) has irrational terms, the following *analytical conditions* have to be satisfied:

- the solutions x_{wi}^C, y_{wi}^C, x_{ri}^C and y_{ri}^C must be real numbers,
- the solutions should not generate complex terms by means of the radicals,
- the solutions of Equation (19) have to be effective solutions of Equations (7) and (8) (they might not be valid due to removal of the radicals by squaring).

Then, for each contact point defined according to the preceding described procedure, the contact forces have to be calculated. The definition of the normal component has been solved using Hertz's theory, while for the tangential force problem, the saturated Kalker theory is used [15].

3.1.3. *MDM roller rig: simulated disturbances*

The objective of this paper is to analyse the performance of the controller and the dynamical behaviour of the MDM roller rig when different kinds of disturbances are coupled with degraded adhesion condition simulation. In this work, the attention was focused on the model uncertainties concerning the geometrical and inertial parameters. The geometrical errors of

the rollers, the errors of the bearing seats and the surface errors can be neglected because the MDM roller rig will be built with high tolerances and the controller is studied to reduce the wear between rollers and wheels. Therefore, the simulated disturbances are as follows:

- *Longitudinal variation*: $\delta G_x(t_0)$ of the position of the centre of mass of the bogie: this disturbance simulates the uncertainty on the bogie position in longitudinal direction when the bogie is positioned on the rollers.
- *Lateral variation* $\delta G_y(t_0)$ *of* the position of the center of mass of the bogie: the introduction of this alteration produces the bogie hunting on the MDM roller rig.
- *Dynamical imbalance of wheelsets and rollers* (δ_M for the mass imbalance, δ_J for the inertial imbalance and δ_G produce an alteration of the positions of the centre of mass of the wheelsets): the dynamical imbalance of the MDM wheelsets/rollers have to be modelled because there are uncertainties in the exact knowledge of the inertial and mass parameters. These effects can disturb the controller performance and stability. In literature there is an European standard referring to the wheelset dynamical imbalance [14].

The dynamical imbalance generates on the wheelset and the roller an approximatively sinusoidal force (at the wheel rotation frequency) that produces a disturbance on the torque estimation. The force *disturbance* modifies the estimated torque $\widetilde{C}_{\mathrm{S}}^{\mathrm{sc}}$ because it alters the estimation of the tangential component of the contact force $\widehat{T}^{\mathrm{sc}}$ as will be explained later in the estimation part. The torque disturbance term can be modelled by the following analytical expression:

$$C_{\mathrm{D}}^{\mathrm{sc}}(t) = A(t)\sin(\hat{\omega}_w(t)t + \phi), \tag{22}$$

where $A(t)$ represents the amplitude approximatively proportional to the centrifugal term, $\hat{\omega}_w(t)$ represents the estimated wheel angular velocity (depending on the work operative condition), ϕ is the phase and it is approximatively constant in time and function of the initial conditions of the system.

The disturbance $C_{\mathrm{D}}^{\mathrm{sc}}(t)$ is defined in the whole work range (in terms of frequency) but its amplitude is variable with the velocity: at low angular speed the error between the real torque and the filtered torque is acceptable while at high angular speed produces vibrations and modifies the dynamical behaviour of the virtual train model.

As demonstrated in practice, it is possible to make a simplifying hypothesis: the *uncoupled spectrum hypothesis*. The spectrum of the torque signal $\tilde{C}_{\mathrm{S}}^{\mathrm{sc}}(t) = \hat{C}_{\mathrm{S}}^{\mathrm{sc}}(t) + C_{\mathrm{D}}^{\mathrm{sc}}(t) + N(t)$ consists of three different contributes: the real torque signal $\hat{C}_{\mathrm{S}}^{\mathrm{sc}}(t)$ (its frequency spectrum is on the left part of Figure 5), the high-frequency noise $N(t)$ (its frequency spectrum is on the right part of Figure 5) and the torque disturbance $C_{\mathrm{D}}^{\mathrm{sc}}(t)$ (its frequency spectrum is in the middle of Figure 5 and it is variable with respect to the wheel angular velocity). If the filter works correctly, the filtered torque $C_{\mathrm{S}}^{\mathrm{sc}}$ coincides with the real torque $C_{\mathrm{S}}^{\mathrm{sc}}$ ($\hat{C}_{\mathrm{S}}^{\mathrm{sc}} = C_{\mathrm{S}}^{\mathrm{sc}}$ in terms of frequency range). In this case, the real torque spectrum has an upper bound of 10 Hz (the real torque range is [0–10] Hz). The upper bound has been evaluated considering the frequency range of both the manual control of the torque and the automatic control of the anti-skid device (ASD) (see Section 3.1.4). Several numerical simulations have been made to verify what happens when the disturbance is present within the real torque range. The results showed that for low speeds the effect of the disturbance is very limited and does not significantly influence the torque estimation. It is then possible to find a lower bound of the imbalance disturbance at a frequency of about 10 Hz. The upper bound of the disturbance range is set to $\cong$ 32 Hz or in other words the maximum wheel angular velocity 200 rad/s. The high frequency noise is produced by dynamical high frequency transients, measure disturbance and numerical noise. In conclusion the situation can be summarised as follows:

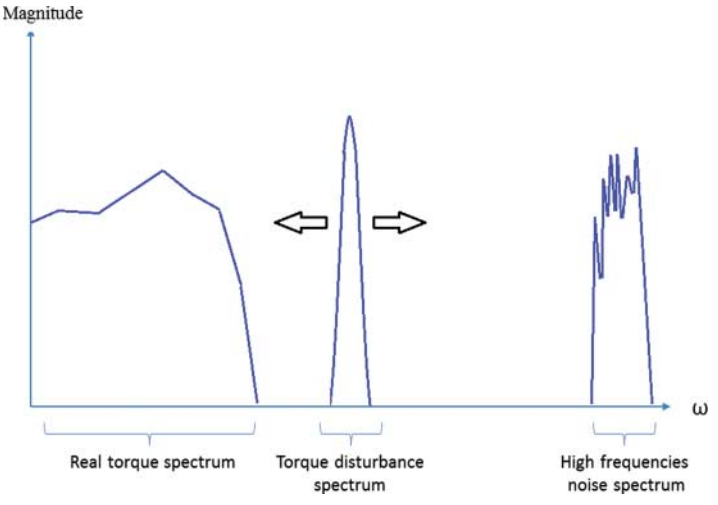

Figure 5. Spectrum of the torque signal.

- real torque $\hat{C}_S^{sc}(t)$ range: [0–10] Hz,
- torque disturbance $C_D^{sc}(t)$ range: [10–32] Hz,
- high-frequency noise $N(t)$ range: over 50 Hz.

3.1.4. *Anti-Skid device*

In order to improve the model of the scaled bogie mounted on the MDM roller rig, an ideal ASD is implemented [18]. The objective of this part was to simulate the behaviour of real antiskid in terms of work frequency and dynamical system. The implementation of a real antiskid system is scheduled as a future development. The anti-slip is an electronic device that allows the reduction of the sliding between wheel and rail in degraded adhesion conditions. This component uses the information about the adhesion state in the virtual train model to calculate the modulated torque that reduces the slidings. The anti-skid works only in a traction phase.

The inputs are the linear velocities ($v = \omega_w r$) and acceleration ($\dot{v} = \dot{\omega}_w r$) of the wheels (where ω_w is the wheel angular speed, $\dot{\omega}_w$ the wheel angular acceleration and r the wheel radius), the motor train torques C^{sc} and the reference values of the virtual train linear velocity and acceleration $\dot{x}, \ddot{x}$ (see Figure 2). The Anti-Skid model uses the information obtained from the virtual train model to define the adhesion states for each wheelsets. The adhesion state is 1 when the wheel loses adhesion and 0 when the wheel is in good adhesion. The outputs of this block are the four modulated torques C_S^{sc}.

The anti-skid model consists of two different parts: the first one, the logic term, evaluates the adhesion state between wheels and rollers comparing the linear velocities and accelerations of the wheels with the virtual train ones; the second one, the action term, defines the strategy to modulate the torque.

The first part of the block includes two criteria used to define the adhesion state between the wheel and roller:

- *Speed criterion*: this criterion compares a threshold value to the velocity error value. This error value is the difference between the linear velocity of the wheels v and the linear velocity $\dot{x}$ of the virtual train.

- *Accelerometer criterion*: this criterion compares the acceleration error value to a threshold value. This error value is obtained by the difference between the linear acceleration $\dot{v}$ of the wheels and the linear acceleration $\ddot{x}$ of the virtual train.

The two criteria use the logical operator OR to produce the activation signal; therefore the sliding condition can also be activated (or deactivated) by one criterion. The logical algorithm of the logical part is

if $[(\dot{v} - \ddot{x}) \geq a_{\text{th}} \vee (v - \dot{x}) \geq v_{\text{th}}]$
then *State of loss adhesion is estimated: State* 1
else *State of full adhesion is estimated: State* 0

The second term defines the action to pass from the loss adhesion State 0 to the full adhesion State 1; to obtain this result the ASD modulates the torque C^{sc} [18]. This block memorises the critical torque $C^{\text{sc}}_{\text{crit}}$ when the State 1 of loss adhesion is revealed (see Figure 6). Starting from this value the torque is reduced using a decreasing ramp ($y = -x$). When the state goes State 0, the torque rises using three different kinds of increasing ramp:

(1) if $C^{\text{sc}} \leq 10\% C^{\text{sc}}_{\text{crit}}$, then the torque increasing ramp is steep ($y = 4x$)
(2) if $10\% C^{\text{sc}}_{\text{crit}} \leq C^{\text{sc}} \leq 70\% C^{\text{sc}}_{\text{crit}}$, then the torque increasing ramp is less steep ($y = 0.4x$)
(3) if $70\% C^{\text{sc}}_{\text{crit}} \leq C^{\text{sc}} \leq 90\% C^{\text{sc}}_{\text{crit}}$, then the torque increasing ramp is slight ($y = 0.15x$)

3.1.5. *Virtual roller rig*

The virtual bogie roller-rig model and the MDM bogie roller-rig model allows the simulation of a full vehicle roller rig [5]. In order to reproduce the dynamics of the whole vehicle, this strategy permits us to physically build only one roller rig (that simulates the front bogie and the half car body) and to simulate via software by means of a simplified model of the roller rig the rest of the wagon. To improve the computational efficiency of the whole system, the virtual roller rig is modelled by a simplified analytical model. This model will be a part of the HIL control system and then will have to run in real time. so it has to be more simple and computationally efficient that those previously described. The input of the block are the rollers control torques $u^{\text{sc}}_3 - u^{\text{sc}}_4$ and the modulated torque C^{sc}_{S} applied by the motors to the

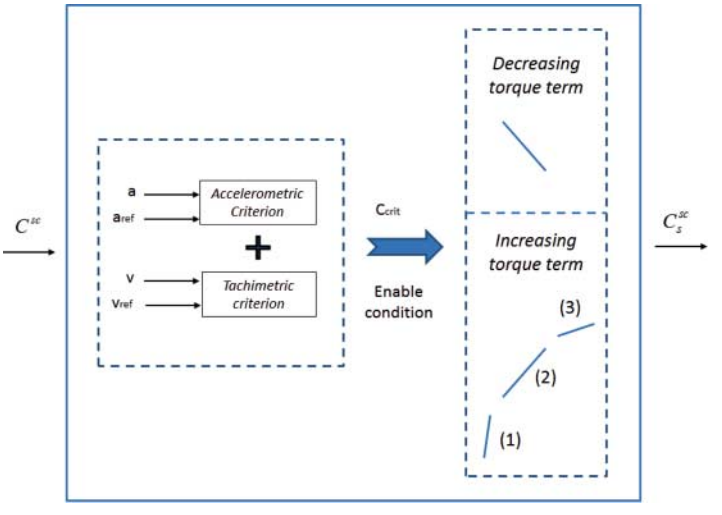

Figure 6. Detailed architecture of the anti-skid device.

wheels (see Figure 2). The output are the same as that of the MDM roller rig: the measured tangential contact force $T_{\text{mis}}^{\text{sc}}$ and the measured roller angular velocity ω_{rm}. The analytical model is simplified with respect to the MDM roller-rig multi-body model because it is based on a two-dimensional dynamical model of a wheelset–roller system.

3.2. *Virtual train model*

3.2.1. *Multi-body model*

The virtual train model permits us to simulate the dynamics of the full-scale railway vehicle. The multi-body model is a simplified two-dimensional model [1] of the longitudinal train dynamics which is used to calculate the linear velocity $\dot{x}_i$, the linear acceleration $\ddot{x}_i$ and the wheelsets load distribution N_i. The goal of the whole system is to simulate the train dynamics in different scenarios: bad adhesion conditions, different physical/geometrical configurations, etc. The train model is bounded in terms of velocity $\dot{x} = \omega_{ws} r$ and motor torque $\hat{C}_{\text{S}}$: the maximum train velocity is approximatively 300 km/h and the maximum motor torque is 20,000 N m (defined by practical observations on the railway vehicles). The inputs of this model are the estimated tangential forces $\widehat{T}$ (estimated by the estimator block and measured from a load cell on the MDM roller-rig support) and the filtered torque $\hat{C}_{\text{S}}$ while the outputs are the reference values of the wheel angular velocity ω_{ws},the simulated tangential force T_{sim}, the train linear velocity $\dot{x}$ and the train linear acceleration $\ddot{x}$ (see Figure 2). The virtual train model uses a simplified adhesion model in order to be implemented directly in real-time software.

As shown in Figure 7, the virtual train model consists of two parts:

- *the train block*: this term simulates the longitudinal dynamics of the train on the rail. The model of the train is composed by a car body, two bogies and four wheelsets; the wheelsets are linked to the bogie by an elastic-viscous force element modelling the primary suspensions while the bogie is connected to the car body by an elastic-viscous element modelling the secondary suspension. This model, from the estimated tangential component force $\widehat{T}$ calculates the longitudinal acceleration $\ddot{x}$ and, imposing equilibrium with respect to pitch rotation, obtains the load distribution N_1, N_2, N_3 and N_4 on the four axles (in Figure 7 the scheme refers to a traction phase).
- *the wheelset block*: this term is a two-dimensional analytic model of the wheelset which calculates the wheel reference angular velocity ω_{ws} and the reference tangential component force T_{sim} starting from the normal component of the load N_i, the linear velocity $\dot{x}$ and the

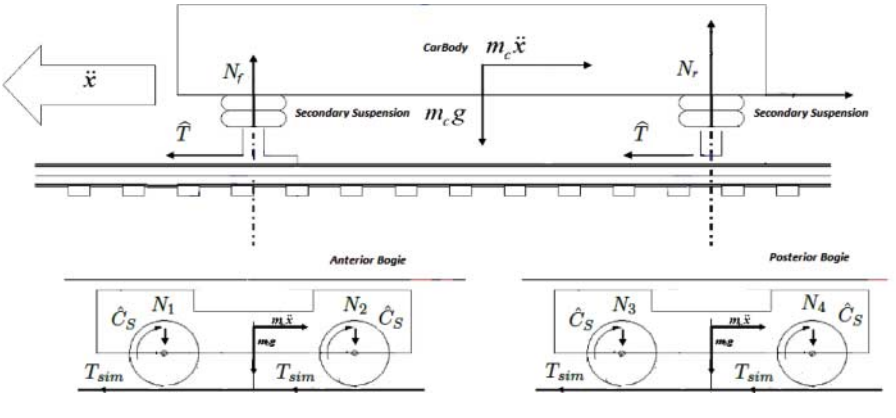

Figure 7. Scheme of the virtual train model.

filtered torque $\hat{C}_S$ (see Figure 2):

$$\dot{\omega}_{ws} = \frac{1}{J}(\hat{C}_S - T_{sim} r), \tag{23a}$$

$$T_{sim} = \mu N, \tag{23b}$$

where μ is the adhesion coefficient calculated from Equation (25), J the axle inertia moment and r the wheel radius.

In the layout of the virtual train model the longitudinal train dynamics and the wheelsets dynamics have been split. This architecture allows us to use in the longitudinal dynamics model the estimated tangential force $\widehat{T}$ calculated by the estimator block (based on the tangential force T_{mis} measured on the MDM roller rig). By means of this strategy, a measured value is introduced in the virtual train model increasing the accuracy of the model. In the development phase also the non-split layout has been tested: in this case, the virtual train model used only a single input, the filtered torque $\hat{C}_S$, because the tangential force T_{sim} evaluated by the wheelset block was directly passed on to the train block. The numerical results showed that the original layout is better in terms of controller performance and noise robustness.

3.2.2. *Simulated adhesion model*

This adhesion model in the virtual vehicle model is needed to simulate the wheel/rail adhesion condition and to tune the roller rig torques in order to simulate the loss and recovery of adhesion of the wheel as discussed in the previous sections. The wheel/rail model presented in this paper is a simplified model able to manage both pure rolling conditions (micro-sliding) and macroscopic sliding. The adhesion model adopted in these preliminary simulations is that described in [4], the research activity in this field is going on and some more accurate models are being developed [19]. Since the aim of the tests described in this paper was to preliminarily evaluate the control performance in presence of external disturbance, in this phase a more simple adhesion model was adopted. In order to implement this model in a real-time software, the model should not be very complicated. The adhesion coefficient μ is positive during the traction phase and negative during the braking phase. First of all, the relative sliding δ is defined by

$$\delta = \begin{cases} \dfrac{r\omega - \dot{x}}{\max(|r\omega|, |\dot{x}|)} & \max(|r\omega|, |\dot{x}|) \neq 0, \\ 0 & r\omega = \dot{x} = 0, \end{cases} \tag{24}$$

where $\dot{x}$ is the linear train velocity, ω the angular velocity of the wheel and r the wheel radius. The adhesion function $\mu(\delta)$ is valid in the range $0 \leq \delta \leq 1$ (see Figure 8) and can be analytically defined as follows:

$$\mu = \begin{cases} -\mu_{asy} - (\mu_0 - \mu_{asy})\, e^{\lambda(\delta+\delta_0)v}, & -1 \leq \delta < -\delta_0, \\ K\delta, & -\delta_0 \leq \delta \leq \delta_0, \\ \mu_{asy} + (\mu_0 - \mu_{asy})\, e^{-\lambda(\delta-\delta_0)r\omega}, & \delta_0 < \delta \leq 1, \end{cases} \tag{25}$$

where μ_0 and μ_{asy} represent the static and the dynamic friction coefficients. These values can be modified in order to simulate different adhesion conditions between the wheel and the rail (for example, including the effects of the environmental conditions).

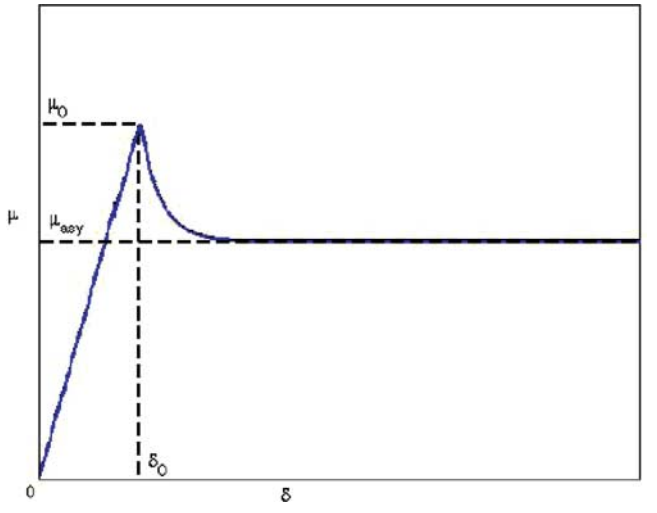

Figure 8. Traction phase: adhesion function.

3.3. *Controller*

The aim of the controller is to reproduce on the roller rig the same values of angular velocity ω_{ws} and accelerations $\dot{\omega}_{ws}$ which have been calculated by the virtual train model [4]. So, it is possible to simulate on the roller rig the same dynamical conditions present in the model. The control action is the roller motor torque. As can be see from the detailed layout of the system, there is one controller for each wheelset. This architecture is studied to give the possibility to recreate different conditions on the four wheelsets.

The control performances are evaluated by means of three parameters:

- *Speed error* e_ω: error between the simulated wheel angular velocity ω_{ws} and the estimated wheel angular velocity $\widehat{\omega}_w$
- *Torque estimation error* e_c: error between the real torque C_S and the filtered torque $\hat{C}_S^{sc} * \phi_C$
- *Control torque* u_i^{sc}: the torques are defined in order to minimise the speed angular error and the torque error between the MDM roller rig and the virtual roller rig.

The input of this block are the simulated tangential forces T_{sim}^{sc}, the simulated wheel angular velocities ω_{ws}, the estimated wheel angular velocities $\widehat{\omega}_w$ and the filtered motor torques $\hat{C}_S^{sc}$. The output are the four control roller torques u_i^{sc} (as shown in Figure 2).

The control torque is the sum of two contributes: the first one (linear) is a feedforward term derived from the dynamical equations of the roller rig and the train model and it is used to generate a control torques that produces on the rig the same wheel angular accelerations calculated by the virtual train model.

The second one is a nonlinear term, defined on the basis of sliding mode control technique [11] and allows us to improve system robustness. This term depends on the difference between the simulated and the estimated wheel angular speed. Furthermore, the nonlinear control torque allows for the compensation of the effects of the inexact knowledge of the real torque C_S and errors in the estimation of dynamic parameters too. For a more detailed description of the roller control refer to [4] for the full-scale and [10] for the scaled one. In conclusion, the total control torque is

$$u_{tot} = u_{cont} + u_{disc}, \tag{26}$$

where u_{cont} and u_{disc} are given by the following equations:

$$u_{\text{cont}} = \frac{R}{r_s}\left(\hat{C}_{\text{S}}^{\text{sc}}\left(1 - \frac{J_B}{J}\phi_T\right) + \frac{J_B}{J}T_{\text{sim}}^{\text{sc}} * \phi_f r\right), \tag{27}$$

$$u_{\text{disc}} = k\text{sign}(\omega_{ws} - \widehat{\omega}_w) \tag{28}$$

in which ω_{ws} represents the simulated angular velocity and $\widehat{\omega}_w$ is the estimated angular velocity.

3.4. *Estimator and filtering*

3.4.1. *Estimator*

The torque applied by the bogie motor to the wheel is not directly measured in order to reduce the number of sensors on the bogie and consequently the time necessary to the setting up phase in the testing activity. The scaled roller rig controller uses as inputs only the roller angular velocity ω_{rm} and the longitudinal component $T_{\text{mis}}^{\text{sc}}$ of the reaction force evaluated on the roller support. The goal of the estimator block is to estimate the wheel angular velocity $\widehat{\omega}_w$, the wheel angular acceleration $\widehat{\dot{\omega}}_w$ and the estimated torque of the wheel motor $\tilde{C}_{\text{S}}$ (see Figure 2). In the MDM roller rig the physical adhesion condition is high and pure rolling conditions between the wheel and the roller can be considered. In this adhesion state, the slidings between wheel and roller can be neglected.

With this hypothesis (supposing that the roller radius is equal to the wheel radius $r_s = R$) the wheel angular velocity, the tangential contact force and the wheel angular acceleration can be estimated as follows:

$$\widehat{\omega}_w = -\omega_{rm}, \quad \widehat{T}^{\text{sc}} = T_{\text{mis}}^{\text{sc}}, \quad \widehat{\dot{\omega}}_w = -\frac{\text{d}}{\text{d}t}\omega_{rm}; \tag{29}$$

where $\widehat{\omega}_w$, $\widehat{T}^{\text{sc}}$ and $\widehat{\dot{\omega}}_w$ are the estimations of the considered quantities. The derivative operation has also to be robust with respect to the numerical noise affecting ω_{rm}. Then, to estimate the wheel motor torque that cannot be directly evaluated, the estimator block uses a simplified dynamical model of the wheel–roller system:

$$\tilde{C}_{\text{S}}^{\text{sc}} = \widehat{T}^{\text{sc}} r_s + J_B \widehat{\dot{\omega}}_w, \tag{30}$$

where r_s is the wheel radius, J_B the total momentum of inertia of the axle/roller system calculated with respect of wheel rotation axis.

3.4.2. *Filter*

A reliable value of the wheel motor torque is fundamental for the control system performance. The torque estimator equation (see Equation (30)) is a function of the wheel estimated angular acceleration $\widehat{\dot{\omega}}_w$ and the estimated tangential contact force $\widehat{T}^{\text{sc}}$. The measured values of ω_{rm} and $\widehat{T}_{\text{mis}}^{\text{sc}}$ (and thus $\widehat{\omega}_w$, $\widehat{\dot{\omega}}_w$ and $\widehat{T}^{\text{sc}}$) can be affected by noise/disturbances that may lead to two problems:

- Influence on the MDM bogie model: the ASD, simulated in the bogie model, uses the train linear velocity $\dot{x}$ and the linear acceleration $\ddot{x}$ to define the modulated torque C_{S} and the values of $\dot{x}$ and $\ddot{x}$ are functions of the estimated torque $\tilde{C}_{\text{S}}^{\text{sc}}$.
- Influence on the virtual train model: the estimated torque $\tilde{C}_{\text{S}}$ defines the dynamical behaviour of the train model. If $\tilde{C}_{\text{S}}$ contains noise/disturbances, then the wheel angular velocity ω_{ws}

and the tangential component of the contact force T_{sim} will be different with respect of those theoretically produced by the real torque C_{S}.

The filter described in this paper is studied to eliminate the particular disturbance $C_{\text{D}}^{\text{sc}}(t)$ and the high-frequency noise $N(t)$, extracting from the estimated torque $\tilde{C}_{\text{S}}^{\text{sc}}$ the filtered torque $\widehat{C}_{\text{S}}^{\text{sc}}$. The filter performance is evaluated by means of the torque estimation error (that is defined by the difference between the real torque C_{S} and the filtered torque $\widehat{C}_{\text{S}}^{\text{sc}} * \phi_C$).

Using the *uncoupled spectrum hypothesis* (previously defined in Section 3.1.3), the disturbance range is fixed; moreover the disturbance is uncoupled with respect to the real torque $\widehat{C}_{\text{S}}^{\text{sc}}$ range and to the noise $N(t)$ range. Therefore, it is possible to set the filter range equal to the range of the disturbance $C_{\text{D}}^{\text{sc}}(t)$ [10–32] Hz.

The analytical form of the torque disturbance (see Section 3.1.3, Equation (22)) approximates the disturbance produced by the dynamical imbalance of the wheelsets and the rollers in the MDM roller rig. In order to decrease the time of the setting up phase, a dynamical identification phase (where the disturbance is exactly evaluated in analytical terms) has not been considered. The filter has been designed in order to operate in real-time, extracting the disturbance $C_{\text{D}}^{\text{sc}}(t)$ from the torque signal $C_{\text{S}}^{\text{sc}}(t)$ and eliminating the disturbance from the torque. As previously explained, the torque signal $\tilde{C}_{\text{S}}^{\text{sc}}$ composed by the sum of three terms:

$$\tilde{C}_{\text{S}}^{\text{sc}}(t) = \hat{C}_{\text{S}}^{\text{sc}}(t) + C_{\text{D}}^{\text{sc}}(t) + N(t). \tag{31}$$

The filtering procedure is schematically sketched in Equation (31): initially, the estimated torque $\tilde{C}_{\text{S}}^{\text{sc}}$ is filtered by a low-pass filter to eliminate the noise $N(t)$. The ideal behaviour of the filter block would be to extract the disturbance $C_{\text{D}}^{\text{scf}}(t)$ without modifying its amplitude A_{CD} and its phase ϕ_{CD} (with respect to $C_{\text{D}}^{\text{sc}}(t)$). The condition $C_{\text{D}}^{s}cf(t) = C_{\text{D}}^{\text{sc}}(t)$ represents one of the main requirement to employ the filter strategy. In this way, the disturbance is eliminated in real-time, obtaining the filtered torque $\hat{C}_{\text{S}}^{\text{sc}}(t)$.

The filter has to fulfil the following requirements:

(1) It has to be computationally efficient for the HIL simulation.
(2) The filtering function has to work in a determinate range of frequencies ([10–32] Hz according to the *uncoupled spectrum hypothesis*); this specification allows for the extraction of the disturbance $C_{\text{D}}^{\text{sc}}(t)$ from the measured torque $\tilde{C}_{\text{S}}^{\text{sc}}(t)$ without modifying the real torque.
(3) The filter transfer function should not modify the amplitude and the phase of the disturbance $C_{\text{D}}^{\text{sc}}(t)$: this characteristic is fundamental in order to apply the strategy defined in Figure 9, since the on-line elimination of the disturbance from the estimated torque $\tilde{C}_{\text{S}}^{\text{sc}}(t)$ is possible only if the $C_{\text{D}}^{\text{scf}}(t)$ has the same amplitude and the same phase of $C_{\text{D}}^{\text{sc}}(t)$.
(4) The filtering function has to be time variant because the disturbance is function of $\hat{\omega}_w(t)$.

The condition (3) can be analytically expressed like amplitude $A_{CD} \cong 1$ and phase $\phi_{CD} \cong 0$; but both conditions are maintained only in a narrow frequency range. Therefore, there are two

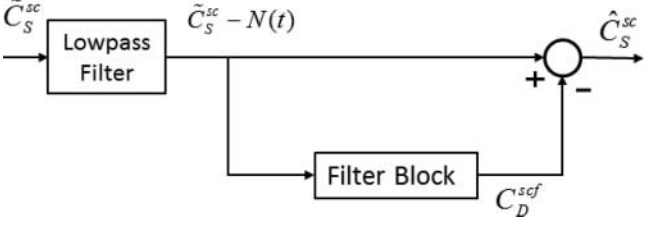

Figure 9. Filter scheme.

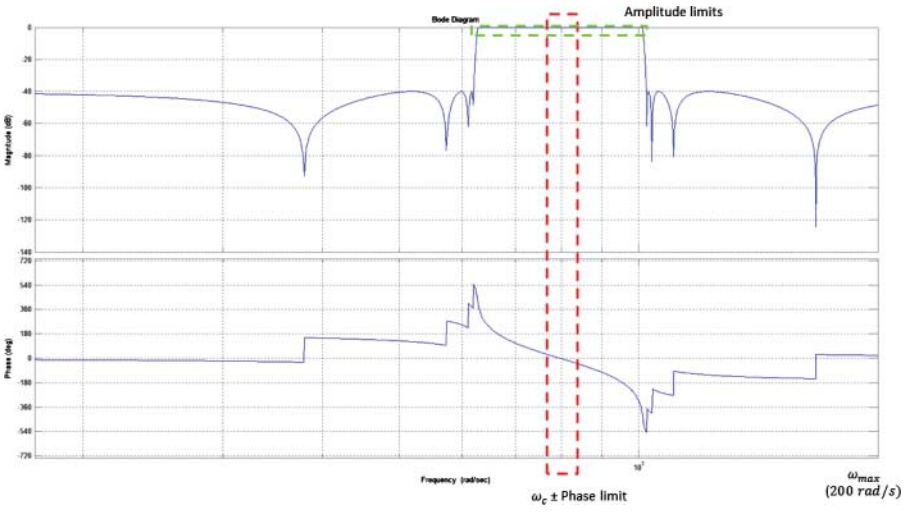

Figure 10. Bode diagram of the *i*th elliptic passband filter: magnitude-phase.

main problems in the filter design: (1) it has to extract $C_{\mathrm{D}}^{\mathrm{sc}}(t)$ respecting the condition (3), (2) it has to be time variant in the whole frequency range [10–32] Hz.

The first part of the problem can be solved using a passband filter that is implemented by means of a sixth-order elliptic filter (since with this filter the performances are reached with medium-low order). The filter band has to respect also the *uncoupled spectrum hypothesis*. In Figure 10, both the no ripple condition $A_{CD} \cong 1$ and the phase condition $\phi_{CD} \cong 0$ can be observed.

As can be seen from the red area and the green area in Figure 10, the conditions required are respected with the selected filter: the amplitude $A_{CD} \cong 1$ and the phase $\phi_{CD} \cong 0$. The problem, as previously said, is the narrow work range where these conditions are respected. The phase condition is more tight than the amplitude condition because only in a very small frequency range the phase is approximately zero. For the phase, we assumed a maximum acceptable value of about $\phi_{CD} \pm 2$ rad/s (*phase limit*), while for the amplitude, we assumed as acceptable the limit $A_{CD} \geq 0.99$.

The problem of the small range (where the phase and the amplitude conditions are respected) can be addressed by discretising the whole frequency range [10–32] Hz in intervals. In this way, it is possible to design every single filter to work in the interval where the phase and the amplitude conditions of the considered filter are verified. The selector block permits us to decide by means of the estimated angular velocity $\hat{\omega}_w$ which filter has to work within its interval. The architecture of this strategy (Multi-state filter) is explained in Figure 11.

The input of the block are the estimated torques $\tilde{C}_{\mathrm{S}}^{\mathrm{sc}}$ and the estimated angular velocity $\hat{\omega}_w$. The output is the filtered torque disturbance $C_D^{\mathrm{scf}}(t)$. The elliptic filter transfer function is defined by

$$G_n(\omega) = \frac{1}{\sqrt{1 + \varepsilon^2 R_n^2(\zeta, \hat{\omega}_w/\omega_0)}}, \tag{32}$$

where R_n is the elliptic rational function with order n, ε represents the ripple factor, ζ the sensitivity factor and ω_0 the cut-off frequency. All these parameters have been set to maintain the amplitude and the phase conditions.

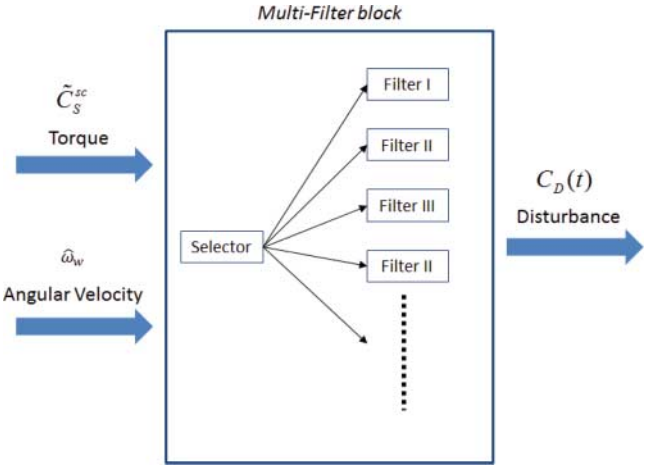

Figure 11. Filter architecture.

Table 2. Parameters of different scenarios.

	Disturbances	Initial conditions	Control parameters
Scenario 1	Bogie lateral offset $\delta G_y(t_0) = 0.0006$ m Low adhesion condition $\mu = 0.05$	$\omega_{\text{init}} = 150$ rad/s Traction Phase	e_c front/rear e_ω front/rear u_i^{sc} $G_y(t)$ $T_{\text{sim}}^{\text{sc}} - T_{\text{cont}\,X}^{\text{sc}} - \widehat{T}^{\text{sc}}$
Scenario 2	Wheelsets imbalance $\delta_M, \delta_J, \delta_G$ Rollers imbalance $\delta_M, \delta_J, \delta_G$ Low adhesion condition $\mu = 0.05$	$\omega_{\text{init}} = 150$ rad/s Traction phase	e_c front/rear e_ω front/rear u_i^{sc} $T_{\text{sim}}^{\text{sc}} - T_{\text{cont}\,X}^{\text{sc}} - \widehat{T}^{\text{sc}}$

4. Numerical simulations

The numerical simulations proposed in this section show the behaviour of the MDM roller rig when virtual degraded adhesion is coupled with different disturbances. The scenarios proposed in this chapter consist in two numerical simulations the characteristics of which are summarised in Table 2.

The parameters used to evaluate the system stability and the controller performance are:

(1) *Speed error* e_ω: error between the simulated angular velocity $\omega_{w_{ws}}$ and the estimated angular velocity $\widehat{\omega}_w$.
(2) *Torque estimation error* e_c: error between the real torque C_S and the filtered torque $\hat{C}_S^{\text{sc}} * \phi_C$. The torque estimation error is referred to as the *full-scale model*.
(3) *Control torque* u_i^{sc}: the torques are defined in order to minimise the speed error and the torque error calculated between the MDM roller rig and the Virtual roller rig. The control torques are referred to as the *scaled model*.
(4) *Lateral displacement* $G_y(t)$: the displacement along the y-axis of the wheelset centre of mass. The displacement is referred to the *scaled model*.
(5) *Creepage forces* $T_{\text{sim}}^{\text{sc}} - \widehat{T}^{\text{sc}} - T_{\text{cont}\,X}^{\text{sc}}$: the creepage force are the tangential component of the contact forces calculated in three cases: the simulated value $T_{\text{sim}}^{\text{sc}}$, the estimated value $\widehat{T}^{\text{sc}}$ and the contact model value $T_{\text{cont}\,X}^{\text{sc}}$. The first one is referred to the virtual train model,

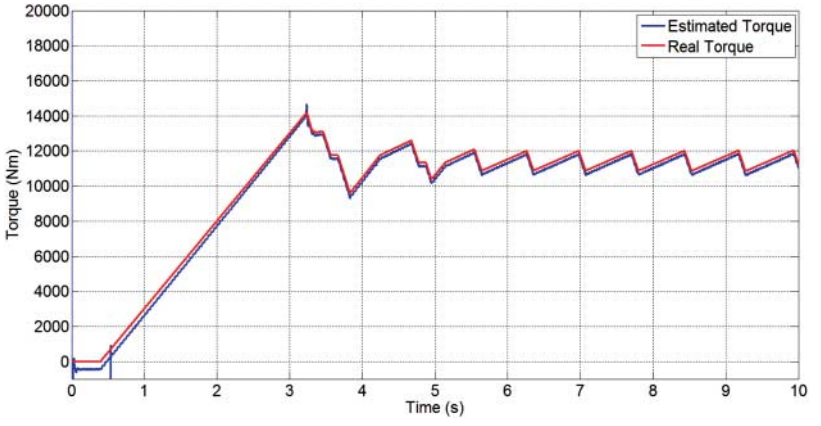

Figure 12. Comparison between the filtered torque $\hat{C}_S^{sc} * \phi_C$ and the real torque C_S on the front wheelset.

the second one is the value estimated by the MDM roller rig estimator and the last one is the value evaluated by the three-dimensional adhesion model. The forces are referred to as the *scaled model*.

The torque in the traction phase is modelled by means of a ramp with an initial delay of 0.5 s, a slope of 5000 N m/s and limited to 20,000 N m. These values are referred to a generic railway vehicle working condition.

4.1. *Scenario 1*

The Scenario 1 objective is to evaluate the control performances and the dynamical behaviour of the MDM roller rig when bad adhesion condition ($\mu = 0.05$) is coupled with a bogie lateral offset ($\delta G_y(t_0) = 0.0006$ m).

The first plot (see Figure 12) shows a comparison between the real torque C_S and the filtered torque $\hat{C}_S^{sc} * \phi_C$ for the front wheelset of the roller rig. In the steady state, the torque error e_c is nearly 0 ± 200 N m, which is acceptable for the requirements of the system, in terms of controller performance and system stability. The controller is then robust in term of torque error. In this graphics the anti-skid behaviour is *also* shown (see Section 3.1.4). The torque rises till the adhesion condition is exceeded. The anti-skid reduces the torque in order to stabilise it around a mean value reducing the sliding between wheel/rig in the virtual train model. Comparing the front and rear wheelset torques, the effects of the traction phase on the longitudinal train model are evident: the load on the rear wheelset is greater than that on the front one. Consequently, the *rear* torque applies on the roller is greater than that on the front one.

The speed error e_ω (see Figure 13), after a transient period, is stabilised at 0.03 rad/s. The controller is also robust in term of speed error. The control torques u_i^{sc} (see Figure 14) follow the torque's behaviour.

The lateral displacements $\delta G_y(t)$ of the wheelset centre of mass (see Figure 15) show that, after a transient period, the displacement converges to zero while the contact forces $T_{sim}^{sc} - T_{cont\,X}^{sc} - \widehat{T}^{sc}$ (see Figure 16) follow the torque behaviour: the forces have the same trend and rise till the maximum value of adhesion. When the anti-skid is activated, the contact forces are stabilised on the value where the adhesion coefficient is maximum. In conclusion, the results show that the controller does not modify the stability of the system and is robust in case of low adhesion condition coupled with a bogie lateral offset (hunting).

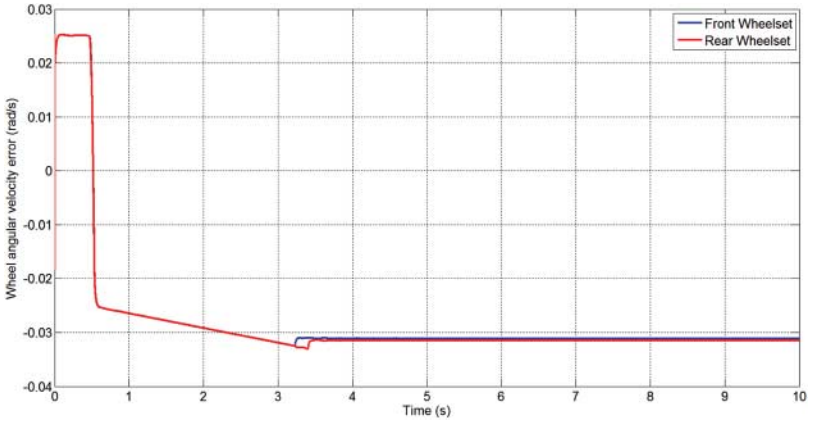

Figure 13. Front/rear speed error e_ω.

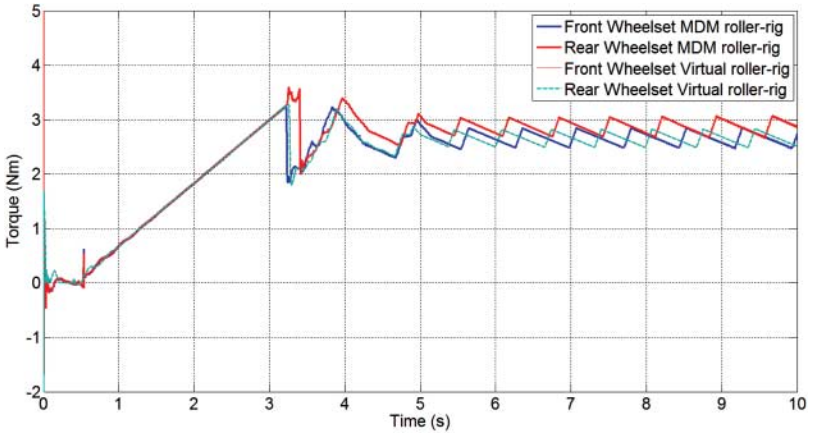

Figure 14. MDM roller rig and virtual roller rig: control torque u_i^{sc}.

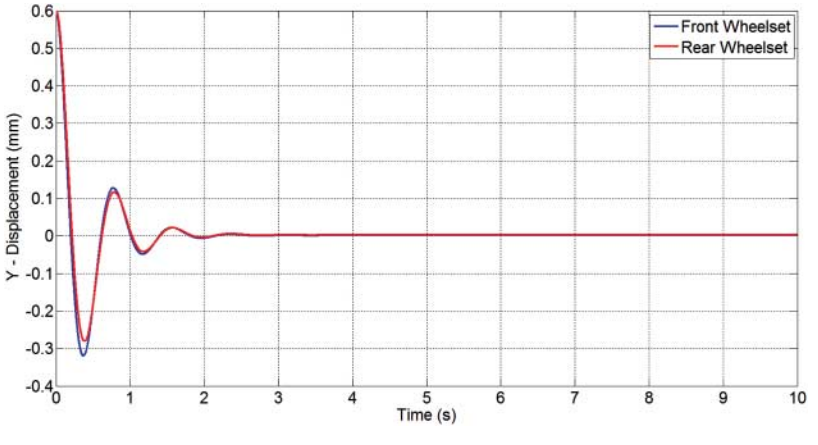

Figure 15. MDM roller rig: front/rear lateral displacements $\delta G_y(t)$.

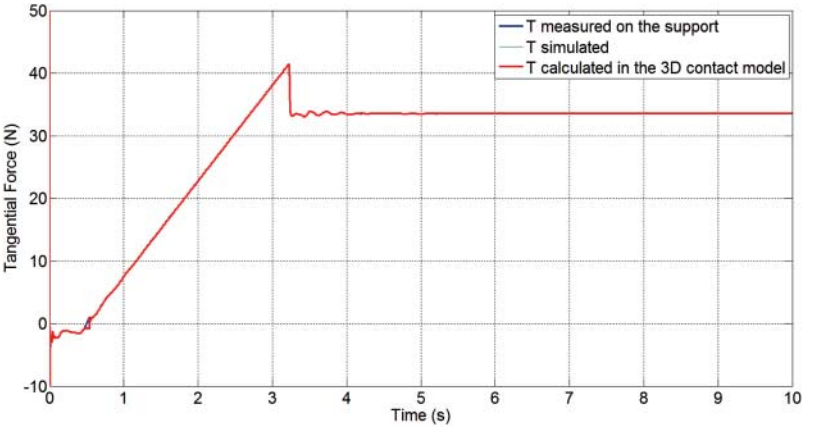

Figure 16. Creepage forces: $T^{sc}_{sim} - T^{sc}_{cont\,X} - \widehat{T}^{sc}$.

4.2. *Scenario 2*

The Scenario 2 shows the dynamical behaviour of the MDM roller rig and the control performances when degraded adhesion condition ($\mu = 0.05$) is coupled with wheelsets/rollers dynamical imbalance [14] δ_M, δ_G and δ_J. In this scenario two different cases are tested: the MDM roller-rig model without Multi-filter and the MDM roller-rig model with Multi-Filter (see Section 3.4.2). The first case allows us to show the effects of the dynamical imbalance on the whole system and the second one permits us to describe the effects of the multi-filter block.

4.2.1. *Dynamical imbalance disturbance without multi-filter*

As can be seen from the graphics, the presence of the dynamical imbalance produces a sinusoidal disturbance on the estimated signal. In Figure 17 the torque behaviour is shown: the real torque C_S follows the Anti-Skid algorithm while in the estimated torque $\tilde{C}^{sc}_S * \phi_C$ the effect of the disturbance $C^{sc}_D(t)$ (see Section 3.4.2, Equation 22) is present.

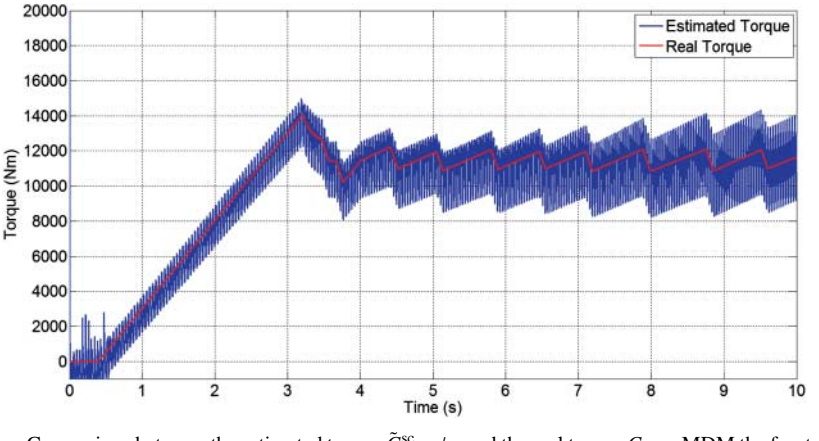

Figure 17. Comparison between the estimated torque $\tilde{C}^{sc}_S * \phi_C$ and the real torque C_S on MDM the front wheelset.

Physically, this disturbance represents a nearly rotating force: several numerical simulations confirmed that a nearly proportional relation between disturbance amplitude $A(t)$ and the centrifugal term exists:

$$A(t) \cong mr\omega^2. \tag{33}$$

The differences are caused by the effect of the three-dimensional adhesion model and the alteration of the inertial tensor δ_J. The minimum torque error e_c is 0 ± 1000 N m and the maximum is 0 ± 2500, which is not acceptable because they are out of range for the requirements of the system, in terms of controller performance and stability system. The controller is not robust in terms of torque estimation error.

The speed error e_ω (see Figure 18) after a transient is stabilised nearly on the same value measured in the scenario 1. This result confirms that the controller is robust in terms of speed error. The control torques u_i^{sc} follows the trend of the torque behaviour (see Figure 19).

The last graphic (see Figure 20) shows the comparison between the contact forces $T_{\text{sim}}^{\text{sc}}$, $\widehat{T}^{\text{sc}}$ and $T_{\text{cont}\,X}^{\text{sc}}$ (see Chapter 3.1.2). Both in the measured tangential force $\widehat{T}^{\text{sc}}$ and the contact force

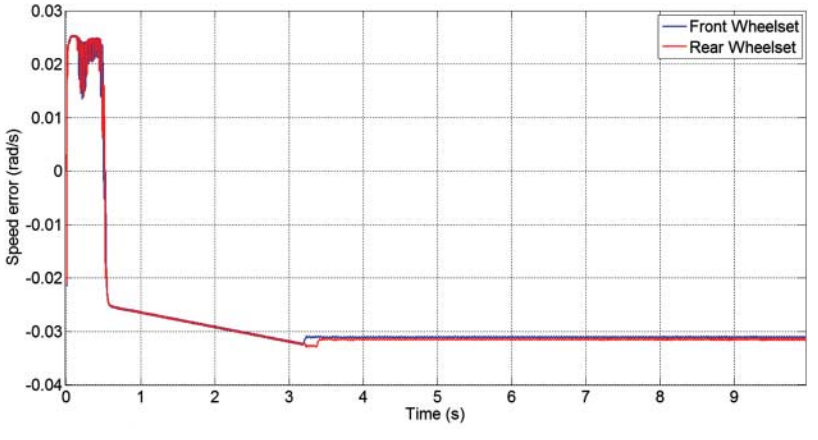

Figure 18. Front/rear speed error e_ω.

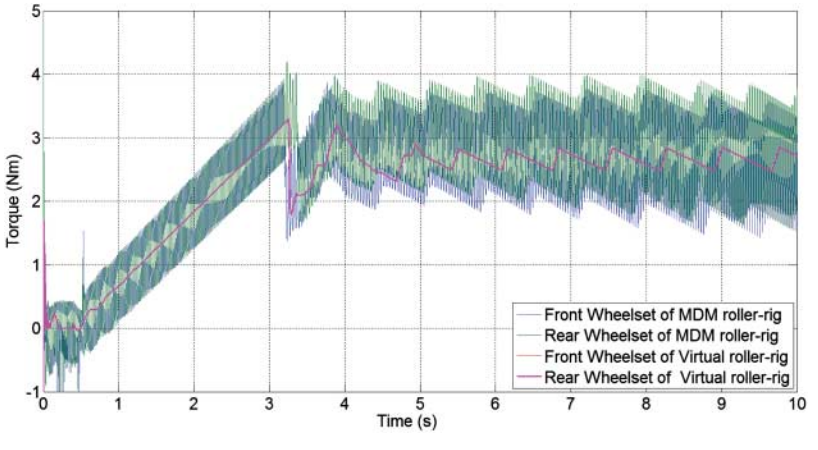

Figure 19. Roller rig and virtual roller rig: control torque u_i^{sc}.

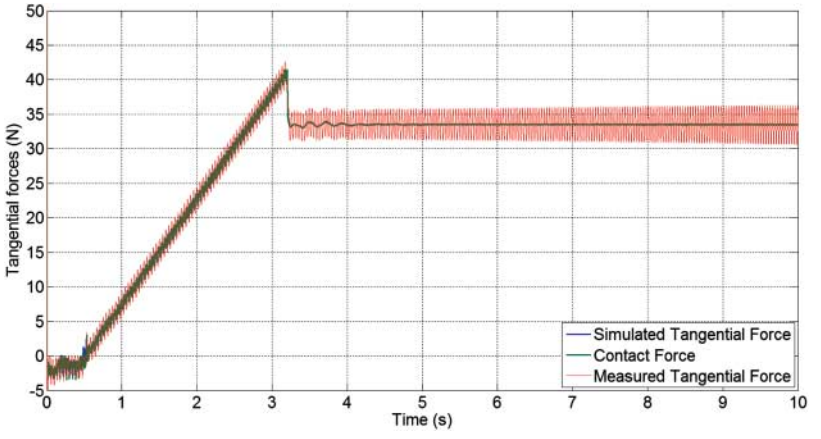

Figure 20. Creepage forces: $T^{sc}_{sim} - T^{sc}_{cont\,X} - \widehat{T}^{sc}$.

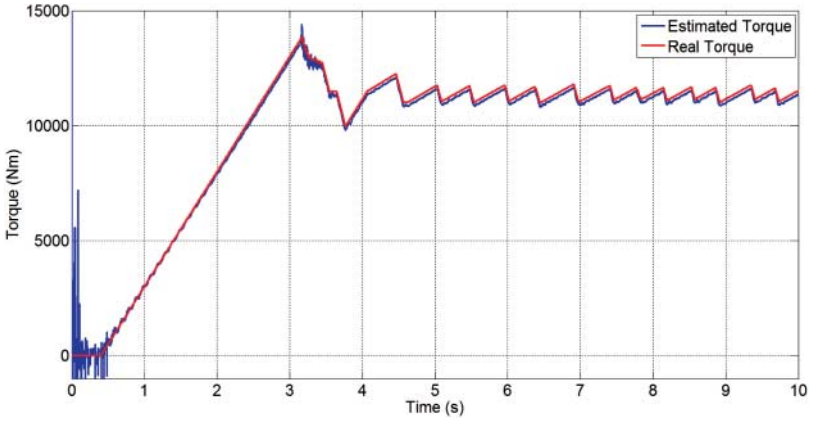

Figure 21. Comparison between the filtered torque $\hat{C}^{sc} * \phi_C$ and the real torque C on the MDM front wheelset.

$T^{sc}_{cont\,X}$ the contribution of the disturbance results evident; while in the simulated tangential force T^{sc}_{sim} the disturbance is not present.

4.2.2. *Dynamical imbalance disturbance with multi-filter*

In this simulation, the filter block (see Section 3.4.2) has been used. The first plot (see Figure 21) shows a comparison between filtered $\hat{C}^{sc}_S * \phi_C$ and real torque C_S on the front wheelsets and the improvement with respect to Figure 17 appears clearly: the disturbance $C^{sc}_D(t)$ is almost completely filtered. The torque error e_c, after the transient period, is ± 300 N m and this result is satisfying (nearly 2.5% of the mean torque value 12,000 N m) as regards the system requirements. The speed error e_ω is included in the range limits (see Figure 22).

The control torque u^{sc}_i of the MDM roller rig and the virtual roller rig follows the torque behaviour (see Figure 23). The comparison between the measured creepage forces $\widehat{T}^{sc}$, the simulated creepage force T^{sc}_{sim} and the calculated creepage force in the contact model $T^{sc}_{cont\,X}$ confirms the presence of the disturbance in two cases only: $\widehat{T}^{sc}$ and $T^{sc}_{cont\,X}$. In the simulated

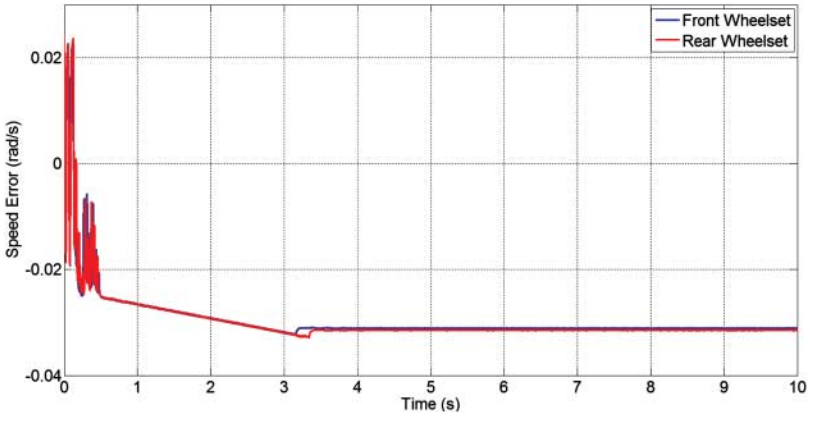

Figure 22. Front/rear speed error e_ω.

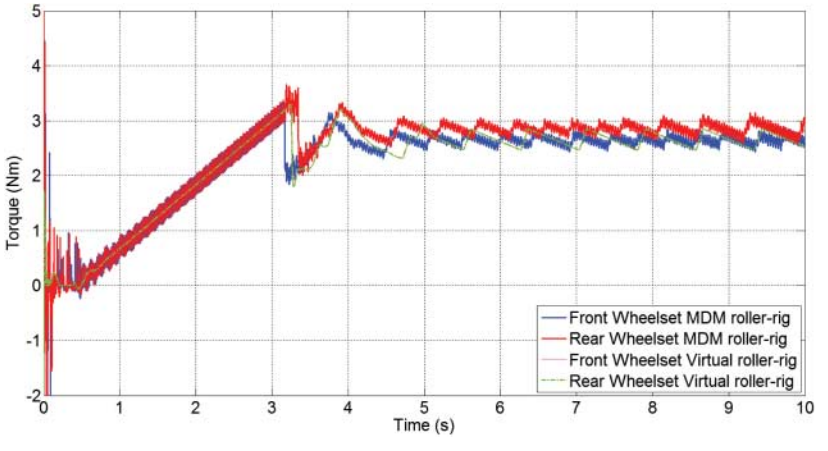

Figure 23. Roller rig and virtual roller rig: control torque u_i^{sc}.

T_{sim}^{sc}, the disturbance effect is very small because this value is directly calculated by the virtual train model where the disturbance is not modelled (Figure 24).

In conclusion:

- the filter block and the controller result are robust in terms of torque estimation error e_c and speed error e_ω,
- the filter block and the controller does not modify the stability of the system,
- the controller is robust and feasible when degraded adhesion condition and dynamical roller/wheel imbalance are coupled.

4.3. *MDM roller rig: numerical performance of the three-dimensional adhesion model developed by MDM lab*

In this section, the numerical performance of whole model (three-dimensional multi-body model of the MDM roller rig and three-dimensional contact model developed by the authors) is investigated. The model performances were analysed comparing with each other the different numerical strategies and focusing on the numerical efficiency of the procedures. In the real

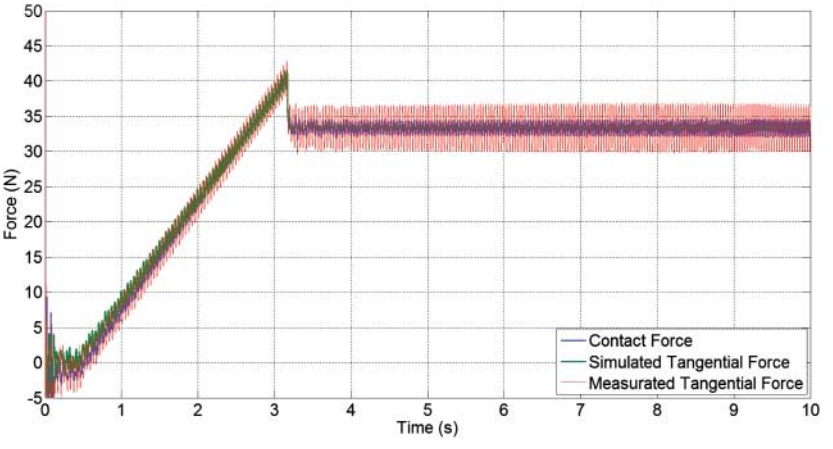

Figure 24. Creepage forces: $T^{sc}_{sim} - T^{sc}_{cont\,X} - \widehat{T}^{sc}$.

Table 3. Comparison between the three different implementation of the contact model in the Simulink® environment.

Type of implementation	Time consuming
MATLAB® function	16.20 h
M-S function	6.20 h
C-S function	25 min

HIL system, the whole model will be replaced by the real MDM scaled roller rig. The main considered MATLAB® structures are:

- MATLAB® function: this kind of structure permits us to use a MATLAB® function (contact model) within Simulink® environment (multi-body model).
- M-S function: this structure allows us to write in MATLAB® script both the parts of the model (multi-body model and contact model).
- C-S function: this kind of structure allows us to write both the parts of the model (multi-body model and contact model) directly in C/C++.

The three implementations are tested in a benchmark case like the 'Scenario 1' where the degraded adhesion condition is coupled with the hunting disturbance. The results are reported in Table 3.

In conclusion, as can be seen in Table 3, the C-S function implementation results very faster than the previous kind of structure.

4.4. *MDM roller rig: Solver parameters*

In this section, the ODE solver used in the MATLAB®-Simulink® environment to optimise the interaction between MDM roller-rig multi-body model and the three-dimensional wheel–roller contact model is described. The choice of these parameters is based on the results upon comparison between several simulations and allows us to obtain a trade-off between the following requirements:

- to ensure the accuracy of the three-dimensional wheel/roller contact model,
- to ensure the accuracy of the multi-body model,
- to reduce the computational load.

The configuration parameters used in the model are summarised in Table 4:

Table 4. Configuration parameters of the Simulink® environment.

Parameters	
ODE solver	ODE 45
Formulation	Runge–Kutta
Type of integration	Variable step
Absolute tolerance	10^{-8}
Relative tolerance	10^{-10}

5. Conclusions and further developments

This paper presented an accurate multi-body model of a scaled roller rig employed within an HIL architecture in order to simulate a scaled railway vehicle test-rig. Since the roller rig is designed to virtually reproduce on the test rig the degraded adhesion conditions, without the physical sliding between the wheel and the roller, the contact model represented a very important part of this model. The contact model described in this paper allows us to consider the fully three-dimensional phenomena and defines a new approach to determine the contact points between two generic revolute surfaces, the wheel and the roller.

The main purpose of this work was to study and analyse the performance of the controller and the dynamic behaviour of the roller rig when different types of disturbances are coupled with degraded adhesion condition, since the effects of the disturbances on the HIL system would degrade the reliability of the simulations. Two different simulation scenarios are presented: Scenario 1 analyses the system when degraded adhesion condition is coupled with bogie hunting, while Scenario 2 studies the system when degraded adhesion condition is coupled with dynamical imbalance. The results of Scenario 1 showed that the controller is robust in terms of speed error and torque estimation error; moreover, in this case the controller does not modify the system stability. On the contrary, when the degraded adhesion condition is coupled with the dynamical imbalance, numerical simulations showed that the system is greatly influenced by the imbalance disturbance, in particular as representing the torque estimation error. The authors proposed a new torque estimation strategy that involves a multi-state filter especially designed to eliminate this particular disturbance. The torque disturbance produced by the dynamical imbalance could be analytically approximated by means of a nearly sinusoidal component. The proposed estimation procedure uses a multi-state filter that allows for the extraction of the sinusoidal disturbance.

The proposed estimation processes were analysed and compared with another estimation procedure previously presented. The numerical simulations showed the effectiveness and robustness of the new torque estimation strategy, both in terms of speed error and torque estimation error. Moreover, the presence of the multi-state filter and the controller does not influence the system stability.

As regards further developments, the comparison between the experimental data coming from physical model of the MDM roller rig and the numerical results is scheduled for the future in order to validate the numerical model. Moreover, also numerical optimisations of the

filter block and of the three-dimensional contact model are planned. The final purpose is to obtain in the MATLAB®–Simulink® environment a complete model of the HIL scheme of the MDM roller rig. This would make possible to realise preliminary tests on the valid numerical model to reduce the time and the economic investments.

Notes

1. These conditions could be replaced by the *orthogonality condition* between the tangent plane to the roller surface in $\mathbf{p}_r^r$ and $\mathbf{d}^r(x_w, y_w, x_r, y_r)$ and the *orthogonality condition* between the tangent plane to the wheel surface in $\mathbf{p}_w^r$ and $\mathbf{d}^r(x_w, y_w, x_r, y_r)$. In this case, this formulation turns out to be analytically more complicated than the previous one and therefore it has not been employed.

References

[1] S. Iwnicki and P. Allen, *Handbook of Railway Vehicle Dynamics*, Vol. Cap 15: Scale Testing, CRC/Taylor & Francis, Boca Raton, FL, 2006.
[2] C. Esveld, *Modern Railway Track*, 2nd ed., Delft University of Technology, The Netherlands, 2001.
[3] L. Pugi, M. Malvezzi, and A. Tarasconi, *Simulations of WSP System on MI-6 Test Rig*, Vehicle Syst. Dynam. 44 (2006), pp. 843–852.
[4] M. Malvezzi, B. Allotta, and L. Pugi, *Feasibility of degraded adhesion tests in a locomotive roller rig*, Proc. Inst. Mech. Eng. Part F 222 (2008), pp. 27–43.
[5] A. Jaschinki, H. Chollet, and S. Iwnicki, *The application of the roller rigs to railway vehicle dynamics*, Vehicle Syst. Dynam. 31 (1999), pp. 345–392.
[6] A. Shabana, M. Tobaa, H. SugiYama, and K. Zaazaa, *On the computer formulations of the wheel/rail contact problem*, Nonlinear Dynam. 40 (2005), pp. 169–193.
[7] M. Malvezzi, E. Meli, J. Auciello, and S. Falomi, *Dynamic simulation of railway vehicles: Wheel–rail contact analysis*, Vehicle Syst. Dynam. 47 (2009), pp. 867–899.
[8] M. Malvezzi, E. Meli, A. Rindi, and S. Falomi, *Determination of wheel–rail contact points with semianalytic method*, Multibody Syst. Dynam. 20 (2008), pp. 327–358.
[9] N. Bosso, A. Gugliotta, and A. Soma', *Progettazione di un banco prova in scala 1/5 per l'analisi sperimentale di carrelli ferroviari*, Proceedings of XXIX congress AIAS, Lucca, Italy, 2000.
[10] B. Allotta, F. Bartolini, L. Pugi, and F. Cangioli, *A scaled roller test rig for high speed vehicles*, Vehicle Syst. Dynam. 48 (2010), pp. 3–18.
[11] J. Slotine and W. Li, *Applied Nonlinear Control*, Prentice-Hall, Englewood Cliffs, NJ, 1991.
[12] Oppenheim, *Discrete-Time Signal Processing*, Prentice-Hall, Englewood Cliffs, NJ, 1989.
[13] S. Iwnicki, *The Manchester Benchmarks for Rail Vehicle Simulators*, Swets & Zeitlinger, Lisse, The Netherlands, 1999.
[14] BS EN 13260:2009+A1:2010, Railway applications. Wheelsets and bogies. Wheelsets. Product requirements, 30 April 2009.
[15] J. Kalker, *Three-dimensional Elastic Bodies in Rolling Contact*, Kluwer Academic Publishers, Dordrecht, The Netherlands, 1990.
[16] O. Polach, *Creep forces in simulations of traction vehicles running on adhesion limit*, Wear 258 (2005), pp. 992–1000.
[17] K. Johnson, *Contact Mechanics*, Cambridge University Press, Cambridge, UK, 1985.
[18] A. Bassi, *Active anti-skidding control strategy on electric locomotives*, Railway Traction System Conference, Capri, Italy, 2001, pp. 87–113.
[19] L. Pugi, A. Ridolfi, M. Malvezzi, F. Cangioli, and A. Rindi, *Three dimensional modelling of wheel–rail degraded adhesion conditions*, 22nd International Symposium on Dynamics of Vehicles on Roads and Tracks, August 14–19, Manchester, UK, 2011.